OPEN

Highly Efficient Bienzyme Functionalized Nanocomposite-Based Microfluidics Biosensor Platform for Biomedical Application

Md. Azahar Ali[1,2], Saurabh Srivastava[1], Pratima R. Solanki[1,5], Venu Reddy[3], Ved V. Agrawal[1], CheolGi Kim[3], Renu John[2] & Bansi D. Malhotra[1,3,4]

[1]Department of Science and Technology Centre on Biomolecular Electronics, Biomedical Instrumentation Section, CSIR-National Physical Laboratory, Dr. K. S. Krishnan Marg, New Delhi-110012, India, [2]Indian Institute of Technology Hyderabad, Ordnance Factory Estate, Yeddumailaram, Hyderabad, Andhra Pradesh 502205, India, [3]Center for NanoBioengineering and SpinTronics, Department of Materials Science and Engineering, Chungnam National University, Daejeon 305-764, South Korea, [4]Department of Biotechnology, Delhi Technological University, Shahbad Daulatpur, Main Bawana Road, Delhi1 110042, India, [5]Special Centre for Nanosciences, Jawaharlal Nehru University, New Delhi-110067, India.

This report describes the fabrication of a novel microfluidics nanobiochip based on a composite comprising of nickel oxide nanoparticles (nNiO) and multiwalled carbon nanotubes (MWCNTs), as well as the chip's use in a biomedical application. This nanocomposite was integrated with polydimethylsiloxane (PDMS) microchannels, which were constructed using the photolithographic technique. A structural and morphological characterization of the fabricated microfluidics chip, which was functionalized with a bienzyme containing cholesterol oxidase (ChOx) and cholesterol esterase (ChEt), was accomplished using X-ray photoelectron spectroscopy (XPS) and scanning electron microscopy. The XPS studies revealed that 9.3% of the carboxyl (COOH) groups present in the nNiO-MWCNT composite are used to form amide bonds with the NH_2 groups of the bienzyme. The response studies on this nanobiochip reveal good reproducibility and selectivity, and a high sensitivity of 2.2 mA/mM/cm². This integrated microfluidics biochip provides a promising low-cost platform for the rapid detection of biomolecules using minute samples.

The ability to monitor desired biomolecules in real time via a microfluidics biochip or a micro-total analytical system (μ-TAS) has aroused considerable interest from the point-of-care (POC) diagnostics community[1,2]. The small geometry of a microfluidics biochip offers many advantages over macroelectrode-based biomedical devices due to its improved mass transport and diffusion, high signal-to-noise ratio, and low detection limit[3,4]. The characteristics of nanocomposites and the intrinsic benefits of microfluidics, including their laminar flow, low consumption of costly reagents and power, portability, minimal need for handling biohazardous materials, fast response time, multiplexing, and parallelization, are advantageous for the fabrication of a biochip[5,6]. The precise liquid control that occurs in a microfluidic platform is essential for the fabrication of microchannels. Polydimethylsiloxane (PDMS) is an attractive polymeric material for the fabrication of microchannels, which can be temporarily sealed with a glass substrate via conformal contact mediated by *Van der Waals* force. Additionally, the hydrophobic properties of PDMS provide good chemical compatibility with organic solvents and cause negligible swelling[5,6].

The microfluidics biochip is known to have many applications, such as enzymatic kinetics and immunoassay analyses; DNA amplification; and cell sorting, culturing, and counting[7]. However, the integration of the microfluidics biochip with a nanostructured material continues to be a challenge. In this context, 1D structures, such as nanotubes, nanowires, and nanocomposites, composed of carbon materials can play an important role in medicinal chemistry and diagnostics, including the creation of biochips for *in vitro* and *in vivo* investigations[3,8–13]. Multiwalled carbon nanotubes (MWCNTs), allotrope of carbon play an important role towards the development of biochips because of their high carrier mobility and tensile strength, as well as their high aspect ratio, which leads to quantum electron transport[12]. In addition, MWCNTs are non-reactive (like graphite) except at the nanotube caps (the tips when they are not cut), where the dangling bonds and edge-plane-like sites located at both ends are
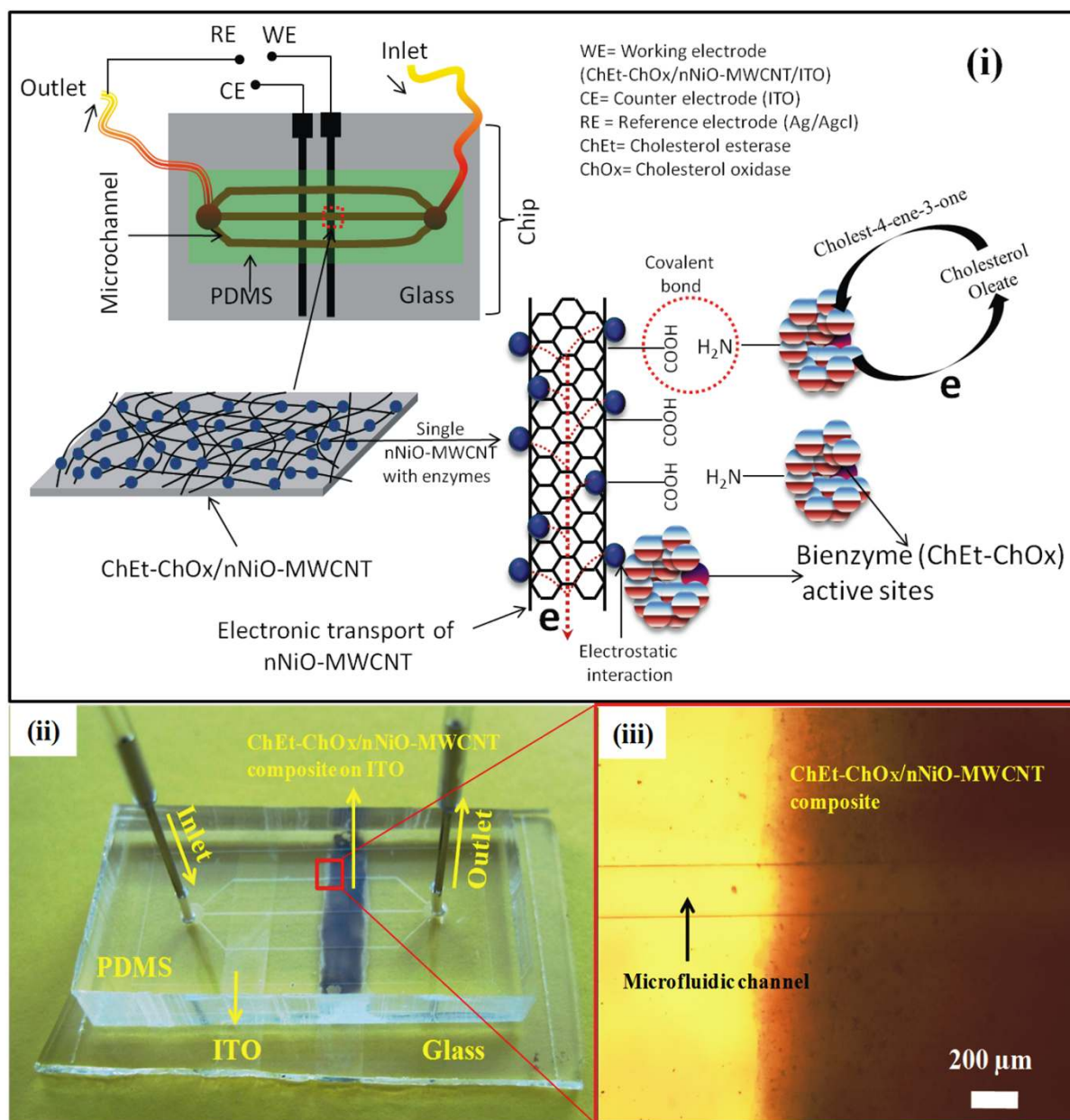
Figure 1 | (i) The schematic of the microfluidic biochip used for total cholesterol detection (the ordered arrangement of this microsystem is assumed). (ii) The photograph of real microfluidic biochip for cholesterol detection and (iii) the enlarged view of optical microscopic image of the microfluidic biochip.

open to reactions[14]. The MWCNTs are known to produce changes in energy bands close to the Fermi level[15,16]. The exciting electronic properties and high electrochemical reactivity of MWCNTs suggest that fast electron transfer reaction occurs when they are used as the electrode in an electrochemical biochip[15,16]. Lin et al. have developed a microfluidics electrochemical sensor for on-site, non-invasive monitoring of lead and chlorophenols[17]. Wisitsoraat et al. have developed an electrochemical biochip for cholesterol detection that has a sensitivity of 0.0512 nA/mg/dl, which is attributed to the direct growth of CNT on glass[18]. However, MWCNTs are known to agglomerate via *Van der Waals* interactions, resulting in poor film-forming ability. To overcome this problem, nanostructured metal oxides (NMOx) may be used to control the agglomeration of MWCNTs[19]. The covalent binding (or sidewall functionalization) of biomolecules (e.g., proteins, enzymes, and nucleic acids) to carboxyl-functionalized MWCNTs via diimide-activated amidation may provide improved stability and reproducibility[20–24]. In such a case, the

large surface area of the MWCNTs and the presence of abundant functional groups may offer a suitable platform for biofunctionalization[20–25]. Additionally, MWCNTs may facilitate continuous conducting pathways to transport the charge carriers, allowing for a higher sensitivity[25]. Shim et al. have used functionalized CNT for biomolecular recognition in a streptavidin/biotin approach to investigate the adsorption of proteins on the sidewalls of carbon nanotubes[20].

A biosensor based on nanostructured nickel oxide (nNiO) has recently been explored to detect biomolecules such as DNA, antibody-antigen interactions, glucose, and cholesterol[26,27]. However, nNiO-based biosensors have limited applications due to the inherently poor electrical conductivity of nNiO[26]. The non-covalent immobilization of enzymes onto nNiO-based biochip has recently been found to result in poor stability of the desired biomolecules[26–28]. To improve the characteristics of a biosensing device, nNiO can be integrated with MWCNTs[29,30]. Zhang et al. have used CNT-NMOx to develop solar cells and gas sensors[21]. The *sp*² hybridization and
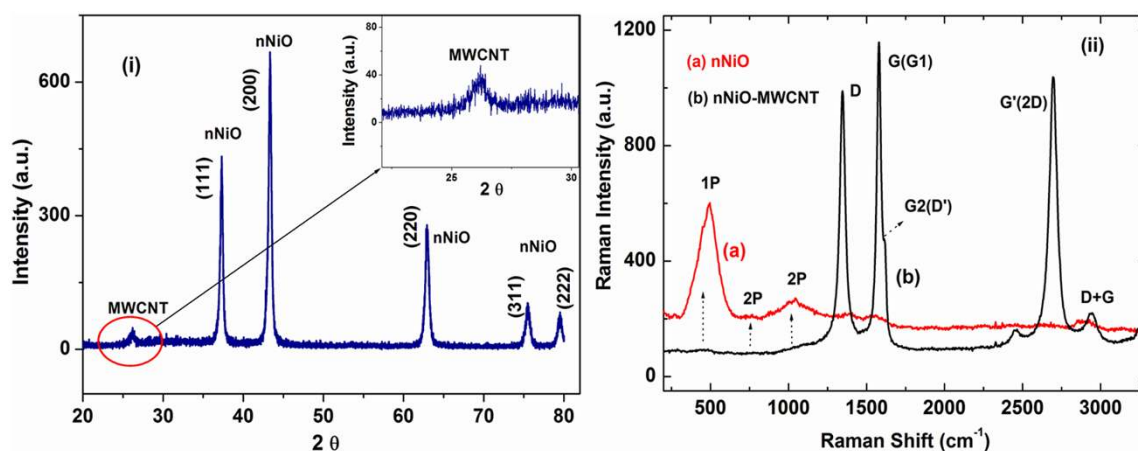
Figure 2 | (i) The X-ray diffraction pattern of nNiO-MWCNTs and (ii) the Raman spectroscopy spectra of the NiO nanoparticles (a) and nNiO-MWCNTs (b).

electronic properties of nNiO coupled with the specific recognition properties of immobilized MWCNTs could lead to a miniaturized biochip[29,30]. Chen et al. have reported the creation of a non-enzymatic electrochemical glucose sensor based on a MnO_2/MWCNT matrix[29]. Zhu et al. have utilized MWCNTs with ZnO nanoparticles for ultra-fast, nonlinear optical switching[19].

In this study, we discuss the fabrication of a novel nNiO-MWCNT nanocomposite-based biochip for total cholesterol estimation. The biochip is immobilized with a bienzyme, composed of cholesterol esterase (ChEt) and cholesterol oxidase (ChOx), and integrated with PDMS microchannels. Unlike conventional methods, our procedure creates bienzyme functionalization through the carboxylation and amidation of the nNiO-MWCNT nanocomposite that serves as the sensing interface.

Results

To confirm the formation of the nanocomposite (nNiO-MWCNT) on the microfluidic electrode, we performed X-ray diffraction (XRD), Raman spectroscopy, X-ray photoelectron spectroscopy (XPS), zeta potential and electrochemical studies. The XRD studies of the nNiO-modified MWCNTs (Fig. 2(i)) revealed the purity and crystallinity of the synthesized NiO nanoparticles with the face-centered cubic configuration (a) (4.1 Å) and space group *Fm3m* (225) (JCPDS Card No. 78-0423). Figure 2(i) reveals a peak at 26° (2θ value) due to the (002) plane (JCPDS Card No. 75-1261) of the MWCNTs. However, the peak intensity of the MWCNTs is lower compared to other peaks due to the presence of defects. The other peaks observed in the diffraction pattern are attributed to the (111), (200), (220), (311), and (222) planes of the cubic NiO[26]. The peak intensity observed for the (200) plane at 2θ (43.3°) is higher than that of the (111) plane, indicating that the growth is mainly dominated by the (200) facet. The d_{200} value of 0.20 nm corresponds to the (200) plane.

The Raman studies (Fig. 2(ii)) show several bands at 532 nm (the excitation wavelength). The vibrational band of NiO (spectra (a)), arising due to one phonon (1P) sampling at 494 cm^{-1}, corresponds to transverse optical (TO) mode. The two-phonon (2P) peak observed at approximately 746 cm^{-1} is assigned to the 2TO and 2LO (longitudinal optical) modes (at approximately 1027 cm^{-1}). The band observed at approximately 713 cm^{-1} exhibits a low intensity at room temperature (298 K), indicating the presence of NiO. In spectra (b), two sharp intense peaks attributed to G (graphite) and D (disorder) bands at 1342 cm^{-1} and 1580 cm^{-1}, respectively, can be observed. The 2D band is found at 2695 cm^{-1} (the second order of the D band). A small feature near 1617 cm^{-1} can be assigned to the G2 or D band, and the peaks pertaining to the G + D band

(approximately 2942 cm^{-1}), as well as a small peak at approximately 2450 cm^{-1}, can also be observed. The tangential G band (approximately 1580 cm^{-1}), derived from the graphite-like in-plane mode, splits into two distinct bands attributed to G1 (1577 cm^{-1}). The G2 (1610 cm^{-1}) peak arises due to changes in the curvature of the inner and outer cylinders.

Figure 3(i) shows an XPS wide-scan spectrum obtained for the nNiO-MWCNT/ITO (subfigure a) and ChEt-ChOx/nNiO-MWCNT/ITO (sub-figure b) electrodes. The peaks found at 284.6 and 530.6 eV are attributed to the C1s and O1s of the COOH-functionalized MWCNTs. In spectrum (b), the characteristic peak observed at 399 eV is attributed to the presence of N1s in the bienzyme (ChEt-ChOx). The additional peaks found at 66.0, 112.6, 777.6, 870.6, and 1009.0 eV are assigned to Ni 3p³, Ni 3S, Ni-Auger, Ni 2p³, and Ni 2P¹, respectively. The Ni 2S peak is due to the incorporation of NiO onto the MWCNTs. The relative atomic concentrations (%) of carbon, nitrogen, oxygen, and nickel are summarized in Table I. The atomic concentration of nitrogen in the ChEt-ChOx/nNiO-MWCNT/ITO bioelectrode was found to be 9.93%. This result indicates that the nNiO-MWCNT/ITO surface facilitates the covalent functionalization of ChEt-ChOx via EDC-NHS chemistry. The XPS spectra of the carbon 1 s region of the deposited nNiO-MWCNT electrode (Fig. 3(ii)) was deconvoluted into characteristic peaks using the Shirley-type baseline and Lorentzian-Doniac-Sunsic curves, with a Gaussian profile. The peak found at 284.1 eV is graphitic (sp^2), the peak at 285.2 eV is due to a defect (sp^3), the peak at 286.3 eV is attributed to a hydroxyl group, the peak at 287.3 eV is assigned to a carbonyl group and the peak found at 288.2 eV is attributed to the carboxyl group (-O-C=O). In the ChEt-ChOx/nNiO-MWCNT/ITO electrode (Fig. 3(iii)), the binding energy peaks corresponding to functional groups are the same as those clearly visible in the spectra of the nNiO-MWCNT/ITO electrode. The observed lower intensities of the ChEt-ChOx electrode, as well as the slight shift in its binding energy positions (Fig. 3(iii)) compared with those of the nNiO-MWCNT/ITO electrode (Fig. 3(ii)), may perhaps be attributed to the covalent attachment of the bienzyme molecules to the film surface. In particular, the COOH group percentage decreased to 2.7% from the nNiO-MWCNT/ITO film's value of 13%, indicating that most of the COOH functional groups are used in bienzyme attachment (ChEt-ChOx). The deconvoluted peak observed at approximately 282 eV in both of the spectra may be due to the adsorption of nNiO to the MWCNTs in the sample. In Figure 3(iv), the typical binding energy peak observed at 398.2 eV is due to the core-level electron of N1s. The peak found at 400.3 eV for the ChEt-ChOx/nNiO-MWCNT bioelectrode corresponds to the amide nitrogen (CO-NH) present in the bienzyme molecules, whereas the peak
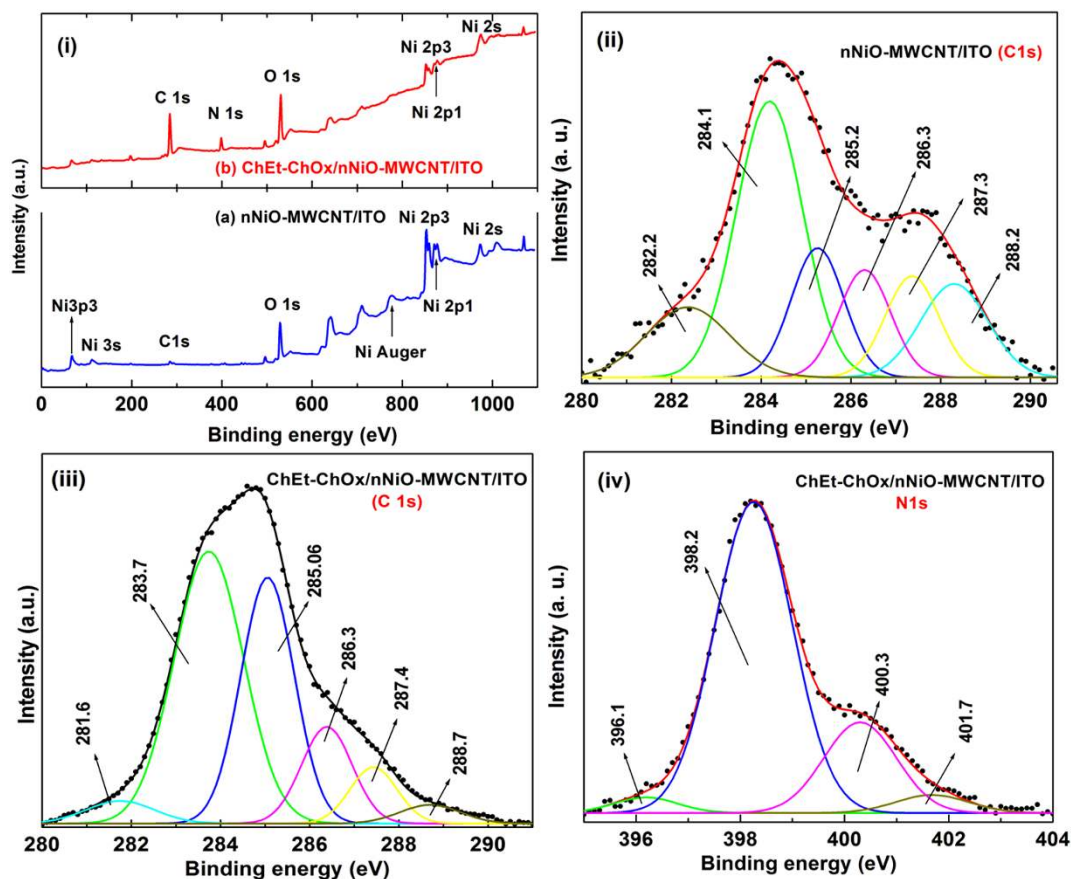
Figure 3 | (i) The wide-scan X-ray photoelectron spectra (XPS) of various films. (ii) The XPS spectra of the C1s region of the nNiO-MWCNT film after deconvolution; (iii) the C1s region of the ChEt-ChOx/nNiO-MWCNT/ITO film; and (iv) the N1s core-level spectra of the ChEt-ChOx/nNiO-MWCNT/ITO film.

observed at 401.7 eV, attributed to the $\equiv$N species, confirms covalent functionalization. The value of the average surface potential of colloidal NiO nanoparticles was estimated to be +22.7 mV using zeta potential measurements. This value reveals that the NiO nanoparticles are positively charged (Supporting Information, Fig. S1(a)). The average surface potential of the MWCNTs was measured to be −6.7 mV, indicating the presence of negatively charged groups on the sidewalls of the carbon nanotubes (Supporting Information, Fig. S1(b)). The positively charged nNiO provides strong electrostatic interactions that link it to the negatively charged MWCNTs.

The scanning electron micrograph (SEM) studies (Fig. S2) were carried out as a morphological observation study at an accelerating voltage of 20 kV. The SEM image (Supporting Information, Fig. S2(i)) shows COOH-functionalized MWCNTs that are likely to be randomly oriented on the ITO substrate. The *in situ* incorporated MWCNTs, with deposited nNiO, are shown in Figure S2(ii). The NiO nanoparticles appear to be attached to the MWCNTs, which are not agglomerated, indicating that the presence of NiO nanoparticles prevented their agglomeration. The transmission electron microscopy (TEM) image shows spherical NiO nanoparticles with an average size of <70 nm (Fig. 4(i)). The high-resolution image of the individual MWCNTs shows outer and inner diameters of 34 and

12 nm, respectively. The selected area electron diffraction (SAED) pattern shows that graphitic (002) and (004) reflections are present in the MWCNTs (the inset in Figure 4(ii)). Figure 4(iii) shows that the well-dispersed COOH-functionalized tubular-shaped MWCNTs are entangled with NiO nanoparticles and randomly oriented. It appears that some of the NiO nanoparticles are aggregated on the MWCNT surfaces. A few NiO nanoparticles can be observed inside the carbon nanotubes (Fig. 4(iii), marked with dotted lines). The length range of the MWCNTs is several tens of micrometers, and they have an external diameter of approximately 20–80 nm. From the atomic-scale image of the nNiO-MWCNTs (Fig. 4(iv)), it can be concluded that this nanocomposite is crystalline in nature, with an interlayer spacing of 3.41 Å (d_{002} for MWCNT, shown in the subfigure inset). The lattice fringe spacing of the NiO nanocrystal is estimated to be 2.0 Å, which agrees with the results of the XRD studies. These results clearly reveal a successful formation of the nNiO-MWCNT composite, which can be used to fabricate the desired biochip.

The electrochemical behavior of the biochip, both before and after undergoing surface modification by the bienzyme (ChEt-ChOx), was investigated using cyclic voltammetry (CV) in phosphate buffer saline (PBS, pH 7.0) containing ferro/ferri cyanide (as a mediator) at a scan rate of 30 mV/s (Fig. 5(A)). The CV of the nNiO/ITO electrode

Table I | The atomic concentration (%) of the elements C, Ni, O, and N present in the nNiO-MWCNT/ITO and ChEt-ChOx/nNiO-MWCNT/ITO films obtained from XPS analysis

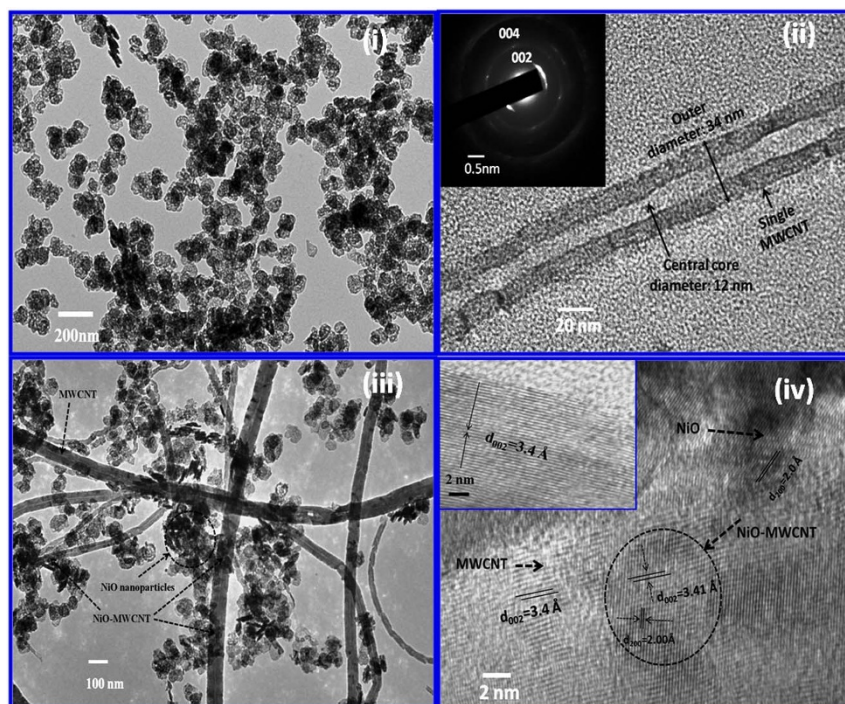| Elements/atomic concentration (%)	C	Ni	O	N
nNiO-MWCNT/ITO	12.52	33.72	53.76	
ChEt-ChOx/nNiO-MWCNT/ITO	59.11	3.88	27.08	9.93

Figure 4 | The HR-TEM analysis of (i) the NiO nanoparticles, (ii) an individual MWCNT (inset: the SAED pattern of the MWCNT), (iii) the MWCNTs modified with NiO nanoparticles, and (iv) an atomic-scale image of a nNiO-MWCNT (inset: lattice fringes of the MWCNT).

exhibited well-defined oxidation/reduction peaks in the -0.8 V to $+0.9$ V potential range, with a peak-to-peak separation (ΔE) of 0.115 V (a). After the nNiO was incorporated into the MWCNTs (1.0%) (b), the electrochemical current increased to 28.0 µA because MWCNTs are more conductive than the nNiO/ITO electrode alone (23.0 µA). The large number of edge plane sites along the surface of the tubes, as well as the presence of defects in the MWCNTs, enhanced the electrochemical behavior. In addition, the outer and inner surfaces of the carbon nanotubes were accessible to the electrolyte solution containing Fe^{3+}/Fe^{2+} ions and became pathways for the transport of electrons toward the electrode, resulting in an enhanced faradic current. In the case of the nNiO-MWCNT(2.0%)/ITO electrode (c), the peak current increased to 31.2 µA. This increase is due to the presence of a large number of defect sites in the MWCNTs, leading to enhanced heterogeneous electron transfer. The resulting current can be controlled by varying the MWCNT concentration in the nNiO matrix. Furthermore, a redox current of 14.0 µA was obtained for the nNiO-MWCNT(2.0%)/ITO electrode after bienzyme functionalization (d), which is lower than that of the nNiO-MWCNT/ITO electrode; the bienzyme has insulating properties that block the transport of electrons toward the electrode. The magnitudes of the cathodic and anodic peaks increased linearly with the square root of the scan rate (30 to 100 mV s^{-1}), indicating a diffusion-controlled or quasi-reversible process and favourable electron transfer kinetics (Supporting Information, Fig. S3). The values of the slope, intercept, and correlation coefficient of the ChEt-ChOx/nNiO-MWCNT/ITO bioelectrode can be estimated using Eq. (1)–(4).

$$I_{pa} = 6.71\ \mu A + 3.55 \left(\mu A m V^{-1} s\right)^{1/2}$$
$$[\text{scan rate (mV/s)}]^{1/2};\ R^2 = 0.999 \quad (1)$$

$$I_{pc} = -0.137\ \mu A - 2.56 \left(\mu A m V^{-1} s\right)^{1/2}$$
$$[\text{scan rate (mV/s)}]^{1/2};\ R^2 = 0.997 \quad (2)$$

$$E_{pa} = 0.368\ V + 1.95\ s^{1/2}\ [\text{scan rate (mV/s)}]^{1/2};\ R^2 = 0.998 \quad (3)$$

$$E_{pc} = -0.235\ V - 1.54\ s^{1/2}\ [\text{scan rate (mV/s)}]^{1/2};\ R^2 = 0.993 \quad (4)$$

The anodic peak potential (E_{pa}) varied linearly with the natural logarithm of the scan rate (ln v) and followed Eq. (5).

$$E_{pa} = 0.232 \ln v + 1.509 \quad (5)$$

The surface concentration of the ChEt-ChOx/nNiO-MWCNT/ITO bioelectrode was estimated using Laviron's theory (Eq. 6), and the slope is given by Eq. (7):

$$RT/\alpha nF = 0.232 \quad (6)$$

$$I_p = n^2 F^2 I^* / 4RT \quad (7)$$

where α is the transfer coefficient, n is the number of electrons transferred (1 in this case), F is the Faraday constant (96485.34 C/mol), I^* is the surface concentration of the ChEt-ChOx/nNiO-MWCNT/ITO bioelectrode, v is the scan rate (mV s^{-1}), R is the gas constant (8.314 J mol^{-1} K^{-1}), and T is the absolute temperature (298 K). The i_p/v value can be calculated from the slope of the i_p versus v plot. The total surface concentration of the ChEt-ChOx/nNiO-MWCNT/ITO bioelectrode was found to be 11.07 $\times$ 10^{-6} mol/cm^2, indicating a high coverage of ChEt-ChOx on the nNiO-MWCNT/ITO surface.

The flow rate was optimized for the ChEt-ChOx/nNiO-MWCNT microfluidics biochip using the chronoamperometric technique (inset of Fig. 5(A)). The chronoamperometric current response of the nNiO-MWCNT/ITO (i) and ChEt-ChOx/nNiO-MWCNT/ITO (ii) electrodes was obtained as a function of the flow rate (0.01–10 µL/min) and the corresponding current versus time, and the plots are shown in Figures S4 and S5 (Supporting Information), respectively. The chronoamperometric current increases for the nNiO-MWCNT/ITO electrode with an increasing buffer solution flow rate. The maximum current is 0.1 µL/min, after which point it reaches
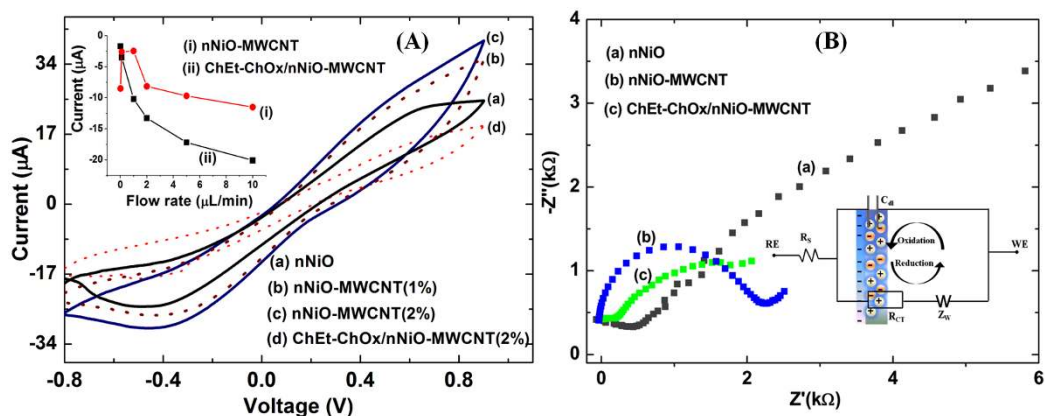
Figure 5 | (A) A cyclic voltammogram (CV) of the different electrodes in a PBS solution (50 mM, pH 7.0, 0.9% NaCl) containing 5 mM of $[Fe(CN)_6]^{3-/4-}$ (inset: current versus flow rate plot of the chronoamperometric response). (B) The electrochemical impedance spectroscopy (EIS) spectra of the electrodes (inset: a schematic representation of the Randles equivalent circuit model for impedance measurement).

saturation (i). This pattern is perhaps due to the diffusivity of the redox species, which increases with a higher buffer flow rate because of the improved mass transport. At a flow rate of 0.1 μL/min, the response time of the microfluidics electrode is 2 s, after which point the amperometric current becomes saturated (Supporting Information, Fig. S4). After its ChEt-ChOx functionalization, the nNiO-MWCNT/ITO electrode (inset of Fig. 5A(ii)) showed a high initial current that decreased as the flow rate increased (Supporting Information, Fig. S5). This response may be attributed to the retention time of the biocatalytic reaction. As the flow rate increases, the retention time becomes shorter, resulting in a decreased response current. It appears that the cholesterol molecules move away from the biochip-sensing surface prior to the completion of the biochemical reaction. The diffusion time was maximized (approximately 3 s) at a flow rate of 1.0 μL/min, so the chronoamperometric measurements were carried out at this optimum flow rate. These results indicate that the fluid flow through the rectangular microchannel is laminar due to the low Reynolds number (0.082).

Electrochemical impedance spectroscopy (EIS) studies were carried out by applying a small-amplitude sinusoidal AC signal (with a bias voltage of 0.35 V) as a function of the frequency (0.01 to 10^5 Hz) (Fig. 5(B)) using a frequency response analyzer (FRA). The electrical impedance (Z) is the ratio of the incremental change in voltage, V(t), to the resulting change in current, I(t), and Z is given by Eq. (8).

$$Z = \frac{V(t)}{I(t)} = \frac{1}{Y} = \frac{V_0 \sin(2\pi ft)}{I_0 \sin(2\pi ft + \varphi)} \tag{8}$$

where V_0 and I_0 are the maximum voltage and current signals, respectively, f is the frequency, t is the time, φ is the phase shift between the voltage-time and current-time function, and Y is the complex admittance. The impedance is described either by the modulus $|Z|$ and the phase shift φ or by its real (Z′) and imaginary (Z″). The most frequently used equivalent circuit for modeling the EIS experimental data is the Randles circuit (inset of Fig. 5(B)), which contains the electrolyte resistance (R_S) in series with a double-layer capacitance (C_{dl}), charge-transfer resistance (R_{CT}), and Warburg impedance (Z_w). The Nyquist plot includes a semicircle region lying on the real axis, which is followed by a straight line. The linear portion ($\varphi = \pi/4$), observed in the low-frequency range, implies a mass-transfer limited process; the semicircle portion, observed in the high-frequency range, implies a charge-transfer-limited process. The imaginary component decreases to zero at a high frequency because it offers no impedance. As the frequency drops, the capacitance (C_{dl}) offers higher impedance and the current flows primarily through the R_{CT} and R_S segments. The R_{CT} value of the nNiO-MWCNT/ITO electrode is 1.9 kΩ (shown in curve b), which is lower than the value of the nNiO/ITO electrode (19 kΩ; curve b). This result is due to the presence of the MWCNTs, which cause enhanced catalytic activity
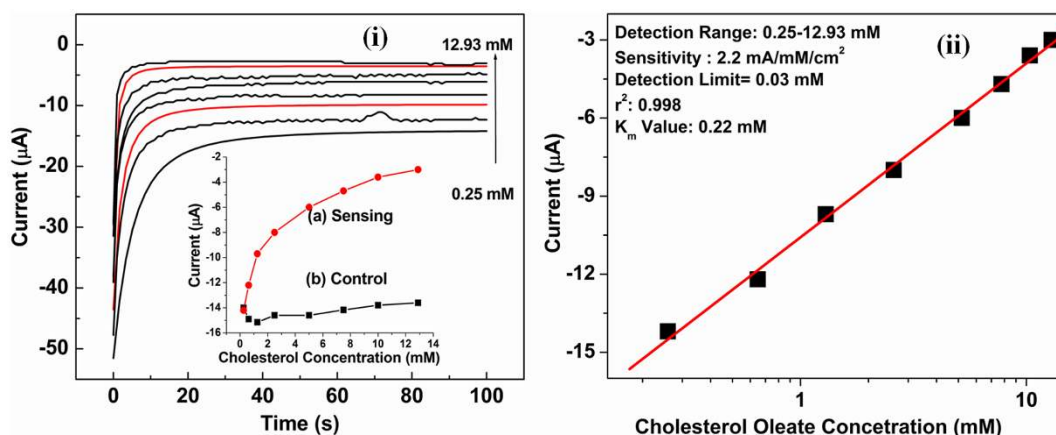

Figure 6 | (i) The chronoamperometric response of the ChEt-ChOx/nNiO-MWCNT/ITO-based biochip as a function of the cholesterol oleate concentration (0.25–12.93 mM) in a PBS solution containing 5 mM of $[Fe(CN)_6]^{3-/4-}$. The experiment was controlled using a syringe pump attached to the inlet of the microsystem (inset: the response current as a function of the cholesterol concentration obtained for both (a) ChEt-ChOx/nNiO-MWCNT/ITO and (b) nNiO-MWCNT/ITO electrodes). (ii) A calibration plot showing the logarithm of the cholesterol concentration (mM) and the amperometric current of the biochip during sensing.
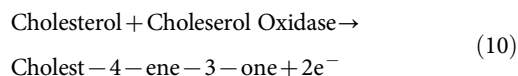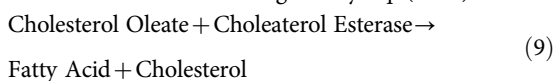
Table II | The sensing characteristics of the nanomaterial-based biochip designed for total cholesterol estimation

Electrode materials	Microfluidic used	Detection limit (M)	Sensitivity (/mM/cm^2)	Detection range	K_m Value (mM)	Stability (days)	Ref.
CNT	Yes	0.25×10^{-3}	0.0512 nA	1.25–10.0 mM	......	......	18
Anatase-TiO$_2$	Yes	1.2×10^{-3}	0.094 mA	0.64–10.3 mM	0.14 mM	35	34
nNiO	Yes	0.65×10^{-3}	0.12 mA	0.64–10.3 mM	0.16 mM	60	26
ZnO	No	37×10^{-9}	23.7 µA	1.0 to 500.0 nM	4.7 mM	50	35
Pt nanoparticles	No	0.2×10^{-6}	2.07 µA	Upto 4.0 µM	5 mM	3	36
Polyelectrolyte-MWCNT	No	0.2×10^{-3}	0.559 µA	Upto 6.0 mM	7.17 mM	......	37
Chitosan/silica-MWCNT	No	1×10^{-6}	1.55 µA	4.0 µM–0.7 mM	0.24 mM	50	33
nNiO-MWCNT	Yes	0.03×10^{-3}	2.2 mA	0.25–12.93 mM	0.22 mM	40	Present Work

and favorable electron-transfer kinetics; improved kinetics leads to a greater diffusion of the $Fe^{2+/3+}$ ions from the bulk solution to the electrode surface. The R_{CT} value of the ChEt-ChOx/nNiO-MW-CNT/ITO bioelectrode increases to 3.9 kΩ (curve c), a value greater than that of the nNiO-MWCNT/ITO (curve b) electrode, implying that the bienzyme absorbed onto the nNiO-MWCNT surface provides steric hindrance to the diffusion of electrons through the electrode-electrolyte interface.

Discussion

The successful formation of the nNiO-MWCNT composite and its bienzyme functionalization were confirmed via XRD, Raman, XPS, SEM, and TEM studies. The chronoamperometric response of the biochip (ChEt-ChOx/nNiO-MWCNT/ITO) was measured (Fig. 6(i)) as a function of the cholesterol oleate concentration (0.25–12.93 mM). During this chronoamperometric measurement, the solutions containing various concentrations of cholesterol oleate in PBS were injected through an inlet of the microchannel at regular intervals. The sensing potential was maintained at −0.4 V during the measurements, when the specific oxidative reaction of the bienzyme ChEt-ChOx was dominant. The chronoamperometric current of the microfluidics biochip increased linearly in the range of 0.25–12.93 mM, after which point it was saturated (inset, Fig. 6(i)a). First, esterified cholesterol was converted into fatty acids and cholesterol in the presence of ChEt. ChOx molecules containing flavin-adenine-dinucleotide (FAD) sites reacted with the cholesterol to produce cholesterol-4-ene-3-one and H_2O_2 via catalytic conversion. The produced H_2O_2 further oxidized to H_2O and oxygen by losing two electrons. These generated electrons (not mediated electrons) are responsible for the enhanced chronoamperometric current that was observed, and the current is directly proportional to the concentration of the injected esterified cholesterol. The enzymatic reactions used for total cholesterol detection are given by Eq. (9–10).

$$\text{Cholesterol Oleate} + \text{Choleaterol Esterase} \rightarrow$$
$$\text{Fatty Acid} + \text{Cholesterol} \tag{9}$$

$$\text{Cholesterol} + \text{Choleserol Oxidase} \rightarrow$$
$$\text{Cholest} - 4 - \text{ene} - 3 - \text{one} + 2e^- \tag{10}$$

A control experiment was conducted using the nNiO-MWCNT/ITO electrode without bienzyme functionalization under similar conditions (inset, Fig. 6(i)b). The current versus time response plot of this control experiment is shown in Figure S5 (Supporting Information). We did not observe any significant change in the current response of the nNiO-MWCNT/ITO electrode with increasing concentrations of esterified cholesterol. These results reveal that the nNiO-MWCNT/ITO electrode surface did not react with the esterified cholesterol molecules, and therefore, the electrochemical current remained unchanged.

Table II shows the characteristics of the fabricated microfluidics biosensor along with those reported in the literature for other devices. It can be observed that the nNiO-MWCNT composite-based microfluidics biodevice exhibits a much higher sensitivity (2.2×10^3 µA/mM/cm^2), lower response time (2 s), lower K_m^{app} (0.22 mM), and more extended linearity (0.25–12.93 mM) than other total cholesterol sensor reported in the literature[33,35–37]. The observed low K_m^{app} value, obtained using the Lineweaver-Burk plot (1/concentration vs. 1/current) and the best linear fit (Table II) indicates that ChEt-ChOx has a high affinity for cholesterol oleate and was properly functionalized onto the nNiO-MWCNT surface. The 20-fold higher sensitivity, 2.2×10^3 µA/mM/cm^2, may be due to the integration of the high-aspect-ratio microfluidics device with the nNiO-MWCNT matrix, as well as an improved biofunctionalization of the bienzyme. The composite material (nNiO-MWCNT) has enhanced electrochemical properties, and the micro-dimensions of the fabricated electrode can cause improved electron diffusion. Additionally, the MWCNTs provide a channel for electron conduction with long electron mean free paths toward the electrode and thus have the capability to support very large current densities. The detection limit of this nanobiochip was found to be a cholesterol concentration of 0.03×10^{-3} M, which corresponds to a physiological range of 2.07–6.2 mM in human blood. The comparatively higher detection limit
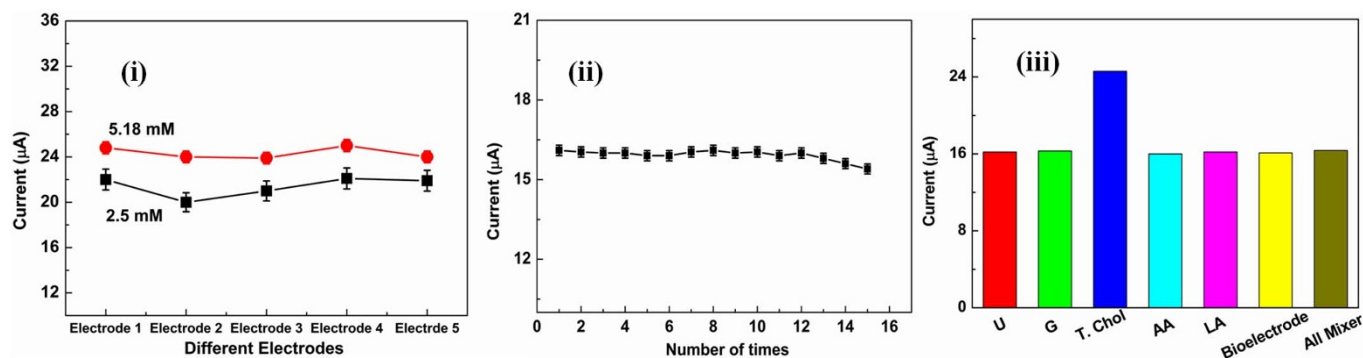

Figure 7 | (i) Reproducibility studies of the ChEt-ChOx/nNiO-MWCNT/ITO microfluidics bioelectrodes under similar conditions. **(ii)** Stability studies of the ChOx-ChEt/nNiO-MWCNT/ITO bioelectrode and **(iii)** selectivity studies of the ChOx-ChEt/nNiO-MWCNT/ITO-based biochip.

of the ChEt-ChOx/nNiO-MWCNT/ITO microfluidics total cholesterol sensor may be caused by either insufficient electrical conductivity of the nNiO or the morphological changes arising as a result of interactions between the bienzyme (ChEt-ChOx) and the nNiO-MWCNT nanocomposite surface[18,26,34,37].

Our biochip shows good reproducibility for cholesterol concentrations of 2.59 and 5.18 mM (Fig. 7(i)) as is evidenced by the low standard deviations (RSD) found (4.19% and 2.13%, n = 5), indicating good precision. The ChEt-ChOx/nNiO-MWCNT/ITO bioelectrode also shows good repeatability, as evidenced by its low RSD of 1.12% (n = 15) for a cholesterol concentration of 2.50 mM. No significant decrease in the current was observed after 12 uses; in further procedures, the bioelectrode showed slight decreases in its current response due to the denaturation of the biomolecules (Fig. 7 (ii)).

The selectivity of the ChEt-ChOx/nNiO-MWCNT/ITO bioelectrode was demonstrated using lactic acid (LA), glucose (G), ascorbic acid (AA), uric acid (UA), and other interferents in a buffer solution. We found that the present bioelectrode is highly specific to total cholesterol (5.18 mM) and shows a negligible change in its response current in the presence of other analytes (interferents) (Fig. 7(iii)). The shelf life of this biochip was determined by measuring the change in the current response at regular 5-day intervals for approximately 3 months; the chip exhibited a 93.7% response after approximately 40 days (data not shown). The ChEt-ChOx/nNiO-MWCNT/ITO bioelectrode was stored at 4°C when not in use. This integrated microfluidics nanobiochip reached 92% of its steady-state current in less than 2 s, indicating that a fast electron exchange was occurring between the active sites of the bienzyme and the nNiO-MWCNT/ITO electrode.

In summary, our miniaturized microfluidics-integrated biochip based on a nNiO-MWCNT composite allows for the rapid detection of biomolecules at a low cost. The nNiO serves as a support for the dispersion of MWCNTs and helps exfoliate smaller bundles or individual nanotubes. The covalent functionalization through reactions of desired chemical groups onto the π-conjugated skeleton of this nNiO-MWCNT composite matrix offers considerable advantages for the development of a nanobiochip to detect molecules such as cholesterol. In particular, the COOH groups on the MWCNTs provide simple biofunctionalization and a higher loading capacity of biomolecules on the microfluidic transducer surface. The 9.3% of the carboxyl groups that were present on the nNiO-MWCNT surface were used to covalently bind with the bienzyme. The synergistic electrocatalytic activity of the MWCNTs provides straight conducting pathways for carriers such as electrons and ions, resulting in a higher sensitivity than nNiO-based biochips. This bienzyme functionalized and integrated microfluidics biochip was highly sensitive to cholesterol oxidation and was both highly reproducible and stable, allowing it to be utilized for total cholesterol monitoring. Our platform exhibits improved detection limits and a faster response time. This highly efficient composite microfluidics biochip could be used to create an array-based biochip that simultaneously monitors multianalytes, including low-density lipoproteins and triglycerides, making it a promising platform for biomedical applications.

Methods

Nickel nitrate [Ni(NO₃)₂]·H₂O and potassium hydroxide (KOH) were procured from Sigma-Aldrich, USA. N-hydroxisuccinide (NHS), N-ethyl-N′-(3-dymethyla-minopropyl carbodiimide) (EDC), cholesterol oxidase (ChOx), cholesterol esterase (ChEt), and cholesterol oleate were purchased from Sigma-Aldrich, USA. Different concentrations of cholesterol oleate, from 0.25 to 12.93 mM, were prepared in 0.9% NaCl solution. SU8-100 negative photoresist and SU-8 developer were purchased from Microchem (Newton, MA, USA).

Instrumentation. The nanostructured nickel oxide (nNiO) and the nNiO-MWCNT matrices were characterized using X-ray diffraction (XRD, Cu Kα radiation, Rigaku), Raman spectroscopy, and transmission electron microscopy (TEM; JEOL JEM-2000 EX). The XPS measurements were performed using an X-ray photoelectron spectrometer (XPS, Multilab 2000, Thermo Scientific) equipped with an alpha 110 hemispherical electron energy analyzer and an X-ray source. The XPS measurements were made in the binding energy range of 0–1100 eV to confirm the ChEt-ChOx functionalization of the nNiO-MWCNT matrix. The electrochemical studies were performed using an electrochemical analyzer (AUT-84275) in PBS at pH 7.0 containing 5 mM of $[Fe(CN)_6]^{3-/4-}$ as a redox species.

PDMS microchannel fabrication. The three rectangular PDMS microchannels were fabricated using the soft lithography technique[26]. The channel height and width were each 200 µm, and the length was 2.0 cm. The microchannels had reservoirs at the end, which were fabricated by punching holes in the PDMS slab at the desired position. The three fabricated channels were connected to reservoirs via a single inlet and outlet (Fig. 1(i)). The principal reason to use three channels is to increase the sensor surface area of the biochip.

Microelectrode fabrication. The indium tin oxide (ITO)-coated glass substrate (with a thickness of approximately 150–300 Å) had a sheet resistance of 70–100 Ω and was used to fabricate the microelectrode (0.6 × 0.26 cm²) via wet chemical etching. The masked ITO was dipped in ITO etchant solution (HNO₃:HCl:H₂O in a 1:10:10 ratio) for 15 min, and ITO was selectively etched from the glass substrate. The ITO electrode was cleaned with acetone and then sonicated with acetone (10 min) and water (2 min) several times. The glass substrate containing the electrodes was hydrolyzed using a mixture of H₂O:H₂O₂:NH₃ (5:1:1) and washed with deionized water. It was then dried in an oven at 100°C for approximately 4 h.

Synthesis of the nNiO-MWCNT composite. The MWCNTs (90%) were synthesized by catalytic chemical vapor deposition using a mixture of ferrocene as the catalyst and toluene as the hydrocarbon source[31]. These MWCNTs were purified and functionalized by refluxing in a concentrated solution of nitric acid and sulfuric acid, which generated a large number of COOH groups on the nanotube surfaces[32]. The drop-wise addition of 0.2 M KOH solution and COOH-terminated MWCNTs to a solution of 0.5 M Ni(NO₃)₂·6H₂O (nickel nitrate) in de-ionized water with constant stirring results in a blackish-green precipitate of nickel hydroxide, Ni(OH)₂, at a pH of approximately 11.8. Excess solvents were evaporated to obtain the precipitate, which was dried at 80°C for 24 h to create a transparent viscous solution of nickel hydroxide-modified MWCNTs. This precipitate was maintained at a pH of 10.0. The thick gel-like Ni(OH)₂-modified MWCNT solution was deposited onto patterned ITO electrodes on the glass substrate via dip coating. The electrodes were initially dried at approximately 110°C for 1 h, and they were then annealed at 400°C under ambient conditions for approximately 2 h to remove any solvent, causing the nNiO-MWCNTs (weight 1.0%) and nNiO-MWCNTs (weight 2.0%) to adhere to the ITO surface.

Functionalization of the bienzyme (ChEt-ChOx). A mixture of ChEt (1 mg/ml) and ChOx (1 mg/ml) in a 1:1 ratio was spread onto the nNiO-MWCNT/ITO microelectrode through physical absorption (Fig. 1(i)); the electrode was then kept in a humid chamber for 4 h at room temperature (298 K). The carboxyl-terminated MWCNTs and the NiO nanoparticles are negatively and positively charged, respectively, resulting in increased electrostatic interactions. However, the carboxylic groups can undergo an amidation reaction with the amino acids of proteins. One approach to covalently bind proteins or enzymes utilizes the diimide-activated amidation of carboxylic acid functionalized carbon nanotubes. The COOH terminal group was activated using EDC (0.4 M) as the coupling agent and NHS (0.1 M) as the activator. The formation of strong covalent (C-N) amide bonds between the COOH groups of the MWCNTs and the NH₂ groups of the bienzyme (Fig. 1(i)) was confirmed via XPS studies. It is possible that the nNiO molecules with a high isoelectric point (an IEP of 10.0) interact with the bienzyme directly through electrostatic interactions due to their low IEP (5.5).

Microfluidics biochip integration. A lithographically fabricated rectangular PDMS microchannel slab was sealed temporarily (irreversible) with the ITO glass substrate using a conformal contact[38] that contained the modified nNiO-MWCNT and ChEt-ChOx electrodes (Fig. 1(i)). The photograph of real microfluidic nanobiochip for cholesterol detection is shown in Fig. 1(ii). Fig. 1(iii) shows the enlarged view of optical microscopic image of this microfluidic nanobiochip. The PDMS surface provides an adhesive layer that plays an important role, making the bonding with the glass substrate irreversible through weak *Van der Waals* forces[38]. Again, the inlet reservoir of the PDMS microchannel was used to introduce the syringe pump, which was based on a stepped motor, to control the fluid flow in the microfluidics biochip. The outlet reservoir was used to accommodate an Ag/AgCl wire that served as the reference electrode (RE). The bare ITO acted as the counter electrode (CE), and the ChEt-ChOx/nNiO-MWCNT/ITO bioelectrode was used as a sensor for total cholesterol detection. All of these three electrodes contained a glass substrate and PDMS microchannels and were embedded on the same biochip.

1. Chován, T. & Guttman, A. Microfabricated devices in biotechnology and biochemical processing. *Trends Biotechnol.* **20**, 116–122 (2002).
2. Hansen, C. & Quake, S. R. Microfluidics in structural biology: smaller, faster. better. *Curr. Opin. Struct. Biol.* **13**, 538–544 (2003).
3. Crevillen, A. G., Avilla, M., Pumera, M., Gonzalez, M. C. & Escarpa, A. Food analysis on microfluidic devices using ultrasensitive carbon nanotubes detectors. *Anal. Chem.* **79**, 7408–7415 (2007).

4. Kim, J., Li, Z. & Park, I. Direct synthesis and integration of functional nanostructures in microfluidic devices. *Lab Chip* **11**, 1946–1951 (2011).

5. Choi, S., Goryll, M., Sin, L. Y. M., Wong, P. K. & Chae, J. Microfluidic-based biosensors toward point-of-care detection of nucleic acids and proteins. *Microfluid. Nanofluid.* **10**, 231–247 (2011).

6. Gervais, L., Rooij, N. & Delamarche, E. Microfluidic chips for point-of-Care immunodiagnostics. *Adv. Mater.* **23**, H151–H176 (2011).

7. Bashir, R. BioMEMS: state-of-the-art in detection, opportunities and prospects. *Adv. Drug. Deliv. Rev.* **56**, 1565–1586 (2004).

8. Wang, J., Chen, G., Wang, M. & Chatrathi, M. P. Carbon-nanotube/copper composite electrodes for capillary electrophoresis microchip detection of carbohydrates. *Analyst* **129**, 512–515 (2004).

9. Fu, Q. & Liu, J. Integrated single-walled carbon nanotube/microfluidic devices for the study of the sensing mechanism of nanotube sensors. *J. Phys. Chem. B* **109**, 13406–13408 (2005).

10. Bange, A., Halsall, H. B. & Heineman, W. R. Microfluidic immunosensor systems. *Biosens. Bioelectron.* **20**, 2488–2503 (2005).

11. Erickson, D. & Li, D. Integrated microfluidic devices. *Anal. Chim. Acta* **507**, 11–26 (2004).

12. Wei, W., Sethuraman, A., Jin, C., Monteiro-Riviere, N. A. & Narayan, R. J. Biological properties of carbon nanotubes. *J. Nanosci. Nanotechnol.* **7**, 1284–97 (2007).

13. Chen, X., Lee, G. S., Zettl, A. & Bertozzi, C. R. Biomimetic engineering of carbon nanotubes by using cell surface mucin mimics. *Angew. Chem. Int. Edn.* **43**, 6111–6 (2004).

14. Balasubramanian, K. & Burghard, M. Chemically functionalized carbon nanotubes. *Small* **1**, 180–192 (2005).

15. Balasubramanian, K. & Burghard, M. Biosensors based on carbon nanotubes. *Anal. Bioanal. Chem.* **385**, 452–468 (2006).

16. Yang, W., Thordarson, P., Gooding, J. J., Ringer, S. P. & Braet, F. Carbon nanotubes for biological and biomedical applications. *Nanotechnology* **18**, 412001 (2007).

17. Lin, Y., Timchalk, C. A., Matson, D. W., Wu, H. & Thrall, K. D. Integrated microfluidics/electrochemical sensor system for monitoring of environmental exposures to lead and chlorophenols. *Biomed. Microdevices* **3**, 331–338 (2001).

18. Wisitsoraat, A. *et al.* Fast cholesterol detection using flow injection microfluidic device with functionalized carbon nanotubes based electrochemical sensor. *Biosens. Bioelectron.* **26**, 1514–1520 (2010).

19. Zhu, Y. *et al.* Multiwalled carbon nanotubes beaded with ZnO nanoparticles for ultrafast nonlinear optical switching. *Adv. Mater.* **18**, 587–592 (2006).

20. Shim, M. *et al.* Functionalization of carbon nanotubes for biocompatibility and biomolecular recognition. *Nano Lett.* **2**, 285–288 (2002).

21. Zhang, W.-D., Xu, B. & Jiang, L.-C. Functional hybrid materials based on carbon nanotubes and metal oxides. *J. Mater. Chem.* **20**, 6383–6391 (2010).

22. Balasubramanian, K. & Burghard, M. Electrochemically functionalized carbon nanotubes for device applications. *J. Mater. Chem.* **18**, 3071–3083 (2008).

23. Tasis, D., Tagmatarchis, N., Bianco, A. & Prato, M. Chemistry of carbon nanotubes. *Chem. Rev.* **106**, 1105–1136 (2006).

24. Katz, E. & Willner, I. Biomolecule-functionalized carbon nanotubes: applications in nanobioelectronics. *ChemPhysChem* **5**, 1085–104 (2004).

25. Vashist, S. K., Zheng, D., Al-Rubeaan, K., Luong, J. H. T. & Sheu, F.-S. Advances in carbon nanotube based electrochemical sensors for bioanalytical applications. *Biotech. Adv.* **29**, 169–188 (2011).

26. Ali, Md. A. *et al.* A highly efficient microfluidic nano biochip based on nanostructured nickel oxide. *Nanoscale* **5**, 2883–2891 (2013).

27. Mohan, S., Srivastava, P., Maheshwari, S. N., Sundar, S. & Prakash, R. Nano-structured nickel oxide based DNA biosensor for detection of visceral leishmaniasis (Kala-azar). *Analyst* **136**, 2845–51 (2011).

28. Solanki, P. R., Kaushik, A., Agrawal, V. V. & Malhotra, B. D. Nanostructured metal oxide-based biosensors. *NPG Asia Materials* **3**, 17–24 (2011).

29. Chen, J., Zhang, W.-D. & Ye, J.-S. Nonenzymatic electrochemical glucose sensor based on MnO$_2$/MWNTs nanocomposite. *Electrochem. Commun.* **10**, 1268–1271 (2008).

30. Zhang, W.-D., Chen, J., Jiang, L.-C., Yu, Y.-X. & Zhang, J.-Q. A highly sensitive nonenzymatic glucose sensor based on NiO-modified multi-walled carbon nanotubes. *Microchim. Acta* **168**, 259–265 (2010).

31. Mathur, R. B., Chaterjee, S. & Singh, B. P. Growth of carbon nanotubes on carbon fibre substrates to produce hybrid/phenolic composites with improved mechanical properties. *Compos. Sci. Technol.* **68**, 1608–1615 (2008).

32. Datsyuk, V. *et al.* Chemical oxidation of multiwalled carbon nanotubes. *Carbon* **46**, 833–840 (2008).

33. Tan, X., Li, M., Cai, P., Luo, L. & Zoua, X. An amperometric cholesterol biosensor based on multiwalled carbon nanotubes and organically modified sol-gel/chitosan hybrid composite film. *Anal. Biochem.* **337**, 111–120 (2005).

34. Ali, Md. A. *et al.* Nanostructured anatase-titanium dioxide based platform for application to microfluidics cholesterol biosensor. *Appl. Phys. Lett.* **101**, 084105 (2012).

35. Umar, A., Rahman, M. M., Vaseem, M. & Hahn, Y.-B. Ultra-sensitive cholesterol biosensor based on low-temperature grown ZnO nanoparticles. *Electrochem. Commun.* **11**, 118–121 (2008).

36. Dey, R. S. & Raj, C. R. Development of an amperometric cholesterol biosensor based on graphene-Pt nanoparticle hybrid material. *J. Phys. Chem. C* **114**, 21427–21433 (2010).

37. Guo, M., Chen, J., Li, J., Nie, L. & Yao, S. Carbon nanotubes-based amperometric cholesterol biosensor fabricated through layer-by-layer technique. *Electroanalysis* **16**, 23 (2004).

38. Kumar, S. *et al.* Microfluidic-integrated biosensors: Prospects for point-of-care diagnostics. *Biotechnol. J.* **8**, DOI 10.1002/biot.201200386 (2013).

Acknowledgements

Author contributions

Md. A.A., R.J. and B.D.M. wrote the manuscript. Md. A.A., S.S. and B.D.M. participated in the experiment design and performance and analyzed the data. S.S. and P.R.S. performed the Raman and HRTEM studies, respectively. V.R. and C.K. carried out the XPS studies. V.V.A., R.J. and B.D.M. supervised the studies and discussed the results. All of the authors reviewed the manuscript and participated in discussions on the results of this research.

Additional information